Size effects in cellular solids

Tekoğlu, Cihan

4 Strain Divergence Theory

In this chapter, we propose a higher-grade continuum theory that treats the divergence of the strains as an independent deformation measure, in addition to the classical strains. We derive the equilibrium equations and the natural boundary conditions. We solve the simple shear and the pure bending problems, and compare the results with the discrete analyses of chapter 2.

4.1 Introduction

The discrete results obtained in Chapter 2 show that a stiffening mechanism is triggered when the cellular materials are subjected to an applied shear deformation. By analyzing the local deformation fields we learned that boundary layers form that are associated with gradients in micro-rotations and shear strains. Another deformation mode that is often associated with deformation gradients and size effects is bending. However, under pure bending the stiffening mechanism was found to be not active. Instead, free-edge effects resulted in overall weakening, which was also observed under uniaxial loading, i.e. in the absence of gradients. Aim of this chapter is to find a generalized continuum theory that is able to pick up the stiffening mechanism under shear, but leaves it inactive under bending.

The stiffening mechanism in the micropolar theory is associated with the gradients in microrotation. These are triggered under shear and when fully coupled to the macroscopic rotations, are able to accurately describe the global (stiffening) and local (boundary layer) response of the discrete microstructures analyzed. However, the same rotation gradients are active under bending as well, erroneously leading to stiffening. Here, we focus on the gradients of strain instead. The particular strain gradient measure should preferably coincide with the shear strain gradient in shear and should be absent in bending. For this, we propose to use the divergence of strain as an additional deformation measure in the theory.

In section 4.2 we derive the equilibrium equations and the natural boundary conditions of the strain divergence theory. In section 4.3, we develop a finite element implementation of the theory. Section 4.4 shows the analytical solution for the simple shear problem and the comparison of the analytical and the discrete results in terms of the macroscopic shear stiffness. In section 4.5, we solve the pure bending problem analytically for the strain divergence theory and finally, in section 4.6, we summarize and discuss the results.

4.2 Strain divergence theory

The deformation measures in strain divergence theory are the conventional strain ε_{ij} and the divergence of strain η_i, defined as

$$\varepsilon_{ij} = \frac{1}{2}\left(u_{j,i} + u_{i,j}\right) \quad \text{and} \quad \eta_i = \varepsilon_{ij,j} = \frac{1}{2}\left(u_{j,ij} + u_{i,jj}\right). \tag{4.1}$$

For a linear elastic, anisotropic material, the strain energy density function can be written as

$$w(\varepsilon_{ij}, \eta_i) = \frac{1}{2} C_{ijkl}\varepsilon_{ij}\varepsilon_{kl} + B_{ijk}\varepsilon_{ij}\eta_k + D_{ij}\eta_i\eta_j, \tag{4.2}$$

where the linear terms in ε_{ij} and η_i are omitted to have zero stress in the undeformed state. Note that in the third term of Equation (4.2), the components of the vector η_k change sign under an inversion of the coordinate system, whereas the components of the tensor ε_{ij} do not. To have an objective strain energy density, B_{ijk} must be a pseudo-tensor (i.e. a tensor whose components change sign under an inversion of the coordinate system). For a material with *central symmetry*, however, the elastic constants must be independent with respect to an inversion of the coordinate system, and this requires the tensor B_{ijk} to vanish (see also section 1.3.1).

The constants D_{ij} are new higher-order constants associated with the divergence of strain η_i, and they have unit of force. The Cauchy stress tensor σ_{ij} and the higher-order stress vector τ_i are work conjugates to the strain tensor ε_{ij} and to the strain divergence vector η_i, and are given as

$$\sigma_{ij} = \frac{\partial w}{\partial \varepsilon_{ij}} = C_{ijkl}\varepsilon_{kl} \quad \text{and} \quad \tau_i = \frac{\partial w}{\partial \eta_i} = 2D_{ij}\eta_j, \tag{4.3}$$

respectively. For an isotropic material, $D_{ij} = a\delta_{ij}$, with "a" being a positive constant. The variation of the total strain energy in a volume V can be written as

$$\delta \int_V w \, \mathrm{d}V = \underbrace{\int_V \sigma_{ij}\delta\varepsilon_{ij} \, \mathrm{d}V}_{I_1} + \underbrace{\int_V \tau_i \delta\eta_i \, \mathrm{d}V}_{I_2}. \tag{4.4}$$

I_1 and I_2 are the parts of the total strain energy density associated with the conventional and higher order terms, respectively. Applying Gauss's divergence theorem, I_1 yields

$$I_1 = \int_S n_i \sigma_{ij}\delta u_j \, \mathrm{d}S - \int_V \sigma_{ij,i}\delta u_j \, \mathrm{d}V, \tag{4.5}$$

where n_i is the outward unit vector normal to the boundary surface S of the volume V. I_2 can be written as

$$I_2 = \frac{1}{2}\left(\underbrace{\int_V \tau_i \delta u_{j,ij}\ \mathrm{d}V}_{P_1} + \underbrace{\int_V \tau_i \delta u_{i,jj}\ \mathrm{d}V}_{P_2} \right). \tag{4.6}$$

Applying Gauss's divergence theorem to P_1 gives

$$P_1 = \underbrace{\int_S n_j \tau_i \delta u_{j,i}\ \mathrm{d}S}_{K_1} - \underbrace{\int_V \tau_{i,j} \delta u_{j,i}\ \mathrm{d}V}_{K_2}. \tag{4.7}$$

Note that if δu_j is already specified on the surface S, the surface part of $\delta u_{j,i}$ cannot be prescribed independently. Therefore, to be able to correctly determine the independent boundary conditions, we decompose the gradient operator into its surface and normal components (see e.g. Mindlin [1964]),

$$\partial_i = D_i + n_i D, \tag{4.8}$$

where the surface gradient operator D_i and the normal gradient operator D are defined as

$$D_i = (\delta_{ij} - n_i n_j)\partial_j \quad \text{and} \quad D = n_k \partial_k, \tag{4.9}$$

respectively. Now we can write K_1 in terms of the components of the gradient vector,

$$K_1 = \int_S [D_i(n_j \tau_i \delta u_j) - D_i(n_j \tau_i)\delta u_j + n_i n_j \tau_i \delta D u_j]\ \mathrm{d}S. \tag{4.10}$$

To further reduce the first term of K_1 we make use of Stokes' surface divergence theorem. This theorem states that the integral of the surface gradient of a continuously differentiable vector function v on a surface S having and edge C, can be written as

$$\int_S D_i v_i\ d\mathrm{S} = \int_S (D_i n_i) n_j v_j\ \mathrm{d}S + \oint_C z_i v_i\ \mathrm{d}s. \tag{4.11}$$

In (4.11), $z_i = \in_{ijk} q_j n_k$ where $\in_{ijk}$ is the Levi-Civita permutation tensor, q_j is the unit tangent vector along the edge C, n_k is the unit normal to the surface S and s is the arc length along C in the direction of q_j. The positive sign of q_j is such that "a man walking along the edge C in the positive q_j direction will find the interior of S to the left, provided his head is in the positive n_k direction" (Malvern [1969]). For the

situation that the volume V has a surface S that consists of m smooth surface segments S_m, with each surface segment having an edge C_m, it follows that

$$\int_S D_i v_i \, \mathrm{d}S = \int_S (D_i n_i) n_j v_j \, \mathrm{d}S + \sum_m \oint_{C_m} z_i v_i \, \mathrm{d}s. \tag{4.12}$$

Figure 4.1, for instance, shows a volume V with a surface S consisting of 32 surface segments S_m (20 hexagons and 12 pentagons). The last term of Equation (4.12) is the

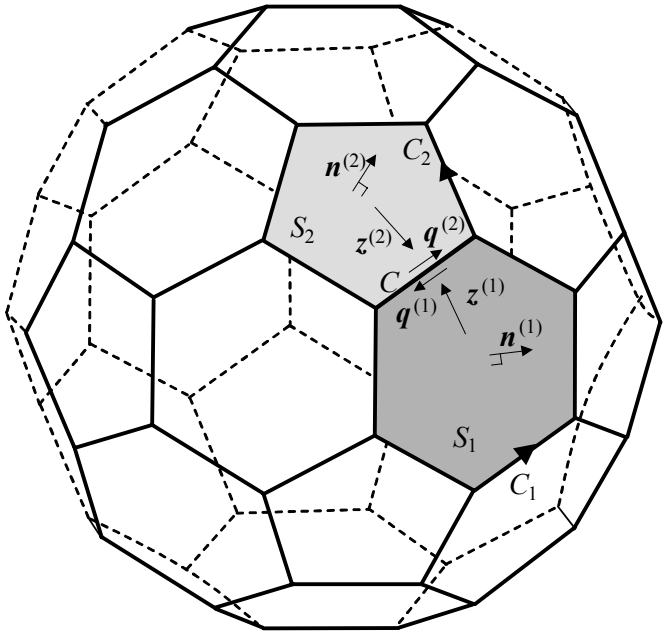

Figure 4.1: Illustration for the positive directions $q^{(1)}$ and $q^{(2)}$ along an edge C with respect to the surfaces S_1 and S_2 to which it is connected.

sum of all integrals over the closed contours C_m. This means that each edge segment C (see Fig. 4.1) has contributions from two contour integrals (over the edges C_1 and C_2 in Fig. 4.1) associated with the two adjacent surface segments S_1 and S_2:

$$\int_C z_i v_i ds = \int_{C_1} z_i^{(1)} v_i \mathrm{d}s^{(1)} + \int_{C_2} z_i^{(2)} v_i \mathrm{d}s^{(2)}. \tag{4.13}$$

By substituting $z_i{}^{(d)} = \in_{ijk} q_j{}^{(d)} n_k{}^{(d)}$, $(d = 1, 2)$ and accounting for the fact that the tangents q_j have opposite directions, $q_j{}^{(2)} \mathrm{d}s^{(2)} = -q_j{}^{(1)} \mathrm{d}s^{(1)}$, the contribution of an edge C to the last term of Equation (4.12) can be written as

$$\int_C \in_{ijk} q_j{}^{(1)} (n_k{}^{(1)} - n_k{}^{(2)}) v_i \, \mathrm{d}s^{(1)} = \int_C \Delta b_i^{(1)} v_i \mathrm{d}s^{(1)}, \tag{4.14}$$

with $\Delta b_i{}^{(1)} = \in_{ijk} q_j{}^{(1)}(n_k{}^{(1)} - n_k{}^{(2)})$. The edge contribution is associated with the jump $\Delta b_i{}^{(1)}$ that vanishes when there are no sharp edges ($n_k{}^{(1)} = n_k{}^{(2)}$). If written in terms of jumps as in Equation (4.14), the contour integrals in Equation (4.12) reduce to line integrals and the summation extends over all line segments (such as C in Fig. 4.1). Here, we will not do so, but continue with the expression in Equation (4.12). Applying Stokes' surface divergence theorem (Equation (4.12)) to the first term of K_1 in Equation (4.10) yields

$$\begin{aligned} K_1 = & \int_S [(D_p n_p) n_i n_j \tau_i - D_i(n_j \tau_i)] \delta u_j \, \mathrm{d}S \\ & + \int_S (n_i n_j \tau_i) \delta D u_j \, \mathrm{d}S + \sum_m \oint_{C_m} z_i n_j \tau_i \delta u_j \mathrm{d}s. \end{aligned} \tag{4.15}$$

By applying Gauss's divergence theorem to K_2 in Equation (4.7), we find

$$K_2 = \int_S n_i \tau_{i,j} \delta u_j \, \mathrm{d}S - \int_V \tau_{i,ji} \delta u_j \, \mathrm{d}V. \tag{4.16}$$

Following the same procedure for P_2 in Equation (4.6), we can write the variation in the total strain energy density as

$$\begin{aligned} \delta \int_V w \, \mathrm{d}V = & -\int_V [\sigma_{ij,i} - \frac{1}{2}(\tau_{i,ji} + \tau_{j,ii})] \delta u_j \, \mathrm{d}V + \\ & \int_S [n_i \{\sigma_{ij} + \frac{1}{2} \left\langle (D_p n_p)(n_j \tau_i + n_i \tau_j) - (\tau_{i,j} + \tau_{j,i}) \right\rangle\} \\ & - \frac{1}{2} D_i(n_j \tau_i + n_i \tau_j)] \delta u_j \, \mathrm{d}S + \\ & \frac{1}{2} \int_S [n_i (n_j \tau_i + n_i \tau_j)] \delta D u_j \, \mathrm{d}S + \\ & \frac{1}{2} \sum_m \oint_{C_m} z_i (n_j \tau_i + n_i \tau_j) \delta u_j \, \mathrm{d}s. \end{aligned} \tag{4.17}$$

The external work done on the body is

$$W^{ex} = \int_V f_j \delta u_j \, \mathrm{d}V + \int_S (t_j \delta u_j + r_j \delta D u_j) \, \mathrm{d}S + \sum_m \oint_{C_m} s_j \delta u_j \, \mathrm{d}s, \tag{4.18}$$

where f_j is the body force per unit volume, t_j is the surface traction, r_j is the higher-order surface traction and s_j is the line force acting over any sharp edge C_m. By

equating the external work done on the body to the internal energy stored, we obtain the equilibrium equations

$$\sigma_{ij,i} - \frac{1}{2}(\tau_{i,ji} + \tau_{j,ii}) + f_j = 0, \tag{4.19}$$

in the volume V, and the boundary conditions on the surface S and along the sharp edges C_m, respectively,

$$n_i\{\sigma_{ij} + \frac{1}{2}\left\langle (D_p n_p)(n_j\tau_i + n_i\tau_j) - (\tau_{i,j} + \tau_{j,i})\right\rangle\} - \frac{1}{2} D_i(n_j\tau_i + n_i\tau_j) = t_j^* \quad \text{or} \quad u_j = u_j^*, \tag{4.20}$$

$$\frac{1}{2} n_i(n_j\tau_i + n_i\tau_j) = r_j^* \quad \text{or} \quad Du_j = Du_j^*,$$

and

$$\frac{1}{2} z_i(n_j\tau_i + n_i\tau_j) = s_j^* \quad \text{or} \quad u_j = u_j^*, \tag{4.21}$$

where the superscript * indicates a prescribed quantity on the surface, or along an edge. Note that the strain divergence theory is a special case of Toupin-Mindlin's strain gradient elasticity: If the four higher-order constants (a_1, a_2, a_4, a_5) in Equation (1.14) vanish, the strain gradient theory reduces to the strain divergence theory, with $a_3 = a$.

4.3 Finite element implementation

To analytically solve the partial differential equations of the strain divergence theory for engineering problems with complex geometries and/or complex loading conditions is a tedious job and even impossible in some cases. Therefore, we will develop a finite element implementation of the strain divergence theory in this section. The strain divergence involves second order gradients of the displacements, which requires C^1-continuous interpolation functions (i.e., both the function and its derivative are continuous at the interface between elements) for the usual displacement-based finite elements. However, there exist no robust C^1-continuous finite elements in the literature for higher order continuum theories (Shu *et al*. [1999], Engel *et al*. [2002]). Hence, we will re-write the virtual work principle in such a form that it is sufficient to use C^0-continuous shape functions. For this purpose, we introduce extra nodal degrees of freedom through a second order tensor ϕ_{ij}, and a related deformation vector $\hat{\eta}_i = (\phi_{ij} + \phi_{ji}),_j/2$. If we strictly enforce the constraint

$$\phi_{ij} = u_{i,j} \tag{4.22}$$

everywhere, then $\hat{\eta}_i$ becomes exactly equal to η_i. In that sense, ϕ_{ij} and $\hat{\eta}_i$ can be referred to as the 'relaxed' displacement gradient and strain divergence, respectively. To enforce this constraint we will use a penalty method. We define an error e_{ij} as

$$e_{ij} = u_{i,j} - \phi_{ij}, \tag{4.23}$$

and a work conjugate penalty measure ρ_{ij} as

$$\rho_{ij} = ke_{ij}, \tag{4.24}$$

where k is the penalty factor. Now, the kinematic constraint (4.22) may be enforced in the volume in an average sense through

$$\int_V \rho_{ij}\delta e_{ij}\ \mathrm{d}V = 0 \quad \text{(no summation on } i \text{ and } j\text{)}, \tag{4.25}$$

which also ensures that the error e_{ij} will be small at the surface. Finally, assuming a smooth surface (so that the line integral at the right hand side of Equation (4.18) vanishes), the virtual work principal may be written, in the absence of body forces, as

$$\int_V (\sigma_{ij}\delta\varepsilon_{ij} + \tau_i\delta\hat{\eta}_i + \rho_{ij}\delta e_{ij})\ \mathrm{d}V = \int_S (t_j\delta u_j + R_{ij}\delta\phi_{ij})\ \mathrm{d}S, \tag{4.26}$$

where $R_{ij} = n_i r_j$. For plane strain loading conditions, the principle of virtual work can be written in vector form as

$$\int_V \delta\boldsymbol{\chi}^{\mathrm{T}}\boldsymbol{\kappa}\ \mathrm{d}V = \int_S \delta\boldsymbol{q}^{\mathrm{T}}\boldsymbol{f}\ \mathrm{d}S, \tag{4.27}$$

where

$$\begin{aligned}
\boldsymbol{\kappa} &= \{\sigma_{11}, \sigma_{22}, \sigma_{12}, \tau_1, \tau_2, \rho_{11}, \rho_{22}, \rho_{12}, \rho_{21}\}^{\mathrm{T}},\\
\boldsymbol{\chi} &= \{\varepsilon_{11}, \varepsilon_{22}, 2\varepsilon_{12}, \hat{\eta}_1, \hat{\eta}_2, e_{11}, e_{22}, e_{12}, e_{21}\}^{\mathrm{T}},\\
\boldsymbol{f} &= \{t_1, t_2, R_{11}, R_{22}, R_{12}, R_{21}\}^{\mathrm{T}},\\
\boldsymbol{q} &= \{u_1, u_2, \phi_{11}, \phi_{22}, \phi_{12}, \phi_{21}\}^{\mathrm{T}}.
\end{aligned} \tag{4.28}$$

$\boldsymbol{\kappa}$, $\boldsymbol{\chi}$, $\boldsymbol{f}$ and $\boldsymbol{q}$ are the generalized stress, generalized strain, generalized traction and nodal degrees of freedom vectors, respectively. The superscript $^{\mathrm{T}}$ indicates the transpose of a matrix or vector. To be able to obtain a unique solution, one has to prescribe four independent boundary conditions on a smooth surface, see Equations (4.17). If the tractions t_j^* and higher order tractions r_j^* on the surface are known, the boundary conditions to be specified for the finite element method are

$$t_j = t_j^* \quad \text{and} \quad R_{ij} = n_i r_j^*. \tag{4.29}$$

Note that for the remainder of this chapter, subscript indices take the values 1 and 2 only. In case of pure displacement loading (u_j^* and Du_j^* are prescribed), we have

$$u_j = u_j^* \quad \text{and} \quad \phi_{ij} = n_j Du_i^* + D_j u_i^*. \tag{4.30}$$

Equation (4.30b) consists of four boundary conditions, of which only two are independently related to Du_j^*. The additional two enforce that the relaxed displacement gradients tangent to the surface are equal to the surface gradients of u_j^*. To make this explicit, we can write

$$\phi_{ij} = (\phi_{ik} n_k) n_j + (\phi_{ik} m_k) m_j, \tag{4.31}$$

where m_i is a unit vector tangent to the surface. Equation (4.30b) is then identical to

$$\phi_{ik} n_k = Du_i^* \text{ and } \phi_{ik} m_k = m_k u_{i,k}^*, \tag{4.32}$$

clearly showing that the first two equations of (4.32) are used to describe the boundary conditions and the second two to complete the constraint $e_{ij} = 0$ at the surface.

Figure 4.2a and b show two triangular elements that we developed for the strain gradient elasticity, to which we refer as the linear and the quadratic element, respectively. The linear element has in total 18 degrees of freedom, six at each node, namely u_1, u_2, ϕ_{11}, ϕ_{22}, ϕ_{12}, ϕ_{21}. The displacements u_i and the relaxed displacement gradients ϕ_{ij} are both interpolated using standard linear shape functions. The generalized strain vector $\boldsymbol{\chi}$ is related to the nodal values of displacements u_i and the relaxed displacement gradients ϕ_{ij} via

$$\boldsymbol{\chi} = LN\boldsymbol{q}^e. \tag{4.33}$$

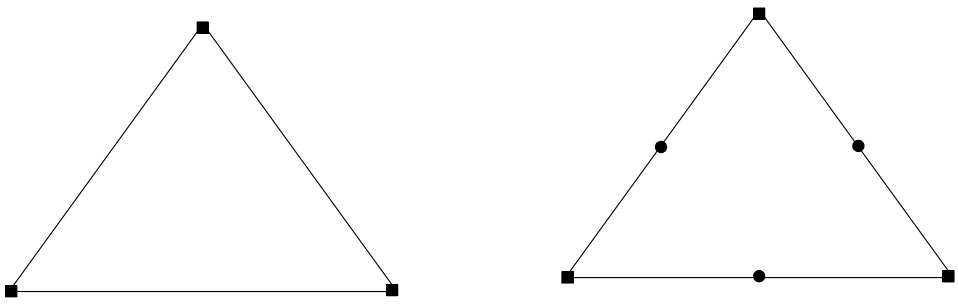

(a) (b)

DOF at ■: $u_1, u_2, \phi_{11}, \phi_{22}, \phi_{12}, \phi_{21}$

DOF at ●: u_1, u_2

Figure 4.2: Sketch of (a) a linear element and (b) a quadratic element.

where L is the differential operator matrix, N is the shape function matrix and $\boldsymbol{q}^e$ is the vector for the 18 nodal degrees of freedom for an element. L is given as

$$L = \begin{bmatrix} \partial/\partial x_1 & 0 & \partial/\partial x_2 & 0 & 0 & \partial/\partial x_1 & 0 & \partial/\partial x_2 & 0 \\ 0 & \partial/\partial x_2 & \partial/\partial x_1 & 0 & 0 & 0 & \partial/\partial x_2 & 0 & \partial/\partial x_1 \\ 0 & 0 & 0 & \partial/\partial x_1 & 0 & -1 & 0 & 0 & 0 \\ 0 & 0 & 0 & 0 & \partial/\partial x_2 & 0 & -1 & 0 & 0 \\ 0 & 0 & 0 & \partial/2\partial x_2 & \partial/2\partial x_1 & 0 & 0 & -1 & 0 \\ 0 & 0 & 0 & \partial/2\partial x_2 & \partial/2\partial x_1 & 0 & 0 & 0 & -1 \end{bmatrix}^T, \quad (4.34)$$

The generalized stress vector $\boldsymbol{\kappa}$ is related to the generalized strains $\boldsymbol{\chi}$ through

$$\boldsymbol{\kappa} = (D_1 + kD_2)\boldsymbol{\chi}, \quad (4.35)$$

where

$$D_1 = \begin{bmatrix} C_{1111} & C_{1122} & & & & & & & \\ C_{1122} & C_{1111} & & & & & & & \\ & & \frac{A^{(1)}_{1212}}{2} & & & & 0 & & \\ & & & 2a & & & & & \\ & & & & 2a & & & & \\ & & & & & 0 & & & \\ & & 0 & & & & 0 & & \\ & & & & & & & 0 & \\ & & & & & & & & 0 \end{bmatrix}, D_2 = \begin{bmatrix} 0 & & & & & & & & \\ & 0 & & & & & & & \\ & & 0 & & & & 0 & & \\ & & & 0 & & & & & \\ & & & & 0 & & & & \\ & & & & & 1 & & & \\ & & 0 & & & & 1 & & \\ & & & & & & & 1 & \\ & & & & & & & & 1 \end{bmatrix}. \quad (4.36)$$

D_1 relates the stress σ_{ij} and the higher order stresses τ_i to the strains ε_{ij} and the strain divergence $\hat{\eta}_i$, and D_2 relates the error e_{ij} to the penalty measure ρ_{ij}. Note that the classical coefficients can be obtained for several cellular microstructures from chapter 3. By substituting Equations (4.33) and (4.35) in the principle of virtual work for one element, Equation (4.27), it follows that

$$\delta \boldsymbol{q}^{e\mathrm{T}} \int_V (B^{\mathrm{T}} D_1 B + k B^{\mathrm{T}} D_2 B)\, \mathrm{d}V \boldsymbol{q}^e = \delta \boldsymbol{q}^{e\mathrm{T}} \int_S N^{\mathrm{T}} \boldsymbol{f}\, \mathrm{d}S, \tag{4.37}$$

where $B = LN$. The discretised equilibrium equations read

$$(K_1{}^e + k K_2{}^e) q^e = K^e q^e = f^e, \tag{4.38}$$

with

$$K_1{}^e = \int_V B^T D_1 B\, \mathrm{d}V \quad \text{and} \quad K_2{}^e = \int_V B^T D_2 B\, \mathrm{d}V. \tag{4.39}$$

$K_1{}^e$ and $K_2{}^e$ form together the stiffness matrix K^e for an element, and they introduce five and four independent relations at each Gauss integration point, respectively.

The linear element (Fig. 4.2a) uses linear shape functions; therefore a patch test for this element must satisfy

$$\begin{aligned} u_i &= A_i + B_i x_1 + C_i x_2, \\ \phi_{ij} &= u_{i,j}, \end{aligned} \tag{4.40}$$

for all possible patches and boundary conditions. In other words, if the values corresponding to the fields given in (4.40) are prescribed at the boundary nodes, the finite element calculations should give the exact values of the displacements u_i and the relaxed displacement gradients ϕ_{ij} for the internal nodes (consistency requirement). We used several different patches containing at least one internal node from which it was concluded that the consistency requirement is satisfied. In addition, to ensure stability, the stiffness matrix for a patch should be non-singular provided that the rigid body modes are eliminated (for a detailed discussion of the patch test, see e.g. Zienkiewicz and Taylor [2000]). If we use a single Gauss integration point for both $K_1{}^e$ and $K_2{}^e$, the total number of independent equations is nine, whereas a single element has thirteen degrees of freedom after subtracting the minimum number of degrees of freedom required to eliminate the rigid body motion. As a result, it fails the stability test. The singularity of the total stiffness matrix disappears for patches with large number of elements. It should be noted that for large patches the element is

susceptible for locking for large values of k, since the stiffness matrix $K_2{}^e$ is non-singular (see e.g. Zienkiewicz and Taylor [2000]).

The quadratic triangular element (see Fig. 4.2b) has six nodes. It has 24 degrees of freedom in total: Each corner node contains all six degrees of freedom (u_1, u_2, ϕ_{11}, ϕ_{22}, ϕ_{12}, ϕ_{21}) and each mid-side node contains only two displacement degrees of freedom (u_1, u_2). Displacements u_i are interpolated using quadratic shape functions and the relaxed displacement gradients ϕ_{ij} are interpolated using standard linear shape functions. For that reason, next to the patch test performed in the case of linear element, we also performed a quadratic patch test, where

$$\begin{aligned} u_i &= A_i + B_i x_1 + C_i x_2 + D_i x_1 x_2 + E_i x_1{}^2 + F_i x_2{}^2, \\ \phi_{ij} &= u_{i,j}. \end{aligned} \tag{4.41}$$

$K_1{}^e$ and $K_2{}^e$ are integrated by three- and one-point Gaussian quadrature, respectively. For several assemblies tested, as well as a single element, the quadratic triangular element satisfies both the consistency and stability requirements of the patch test. In addition, $K_2{}^e$ is singular, so that locking will not occur when k becomes large.

In the next section, we will show the convergence for the linear and quadratic elements by comparing the finite element calculations with the analytical solution for the simple shear problem.

4.4 Analytical solution of the simple shear problem

Figure 4.3 shows the boundary conditions of the simple shear problem for the strain divergence theory in plane strain. In addition to the displacement boundary conditions corresponding to the classical problem, we specify the higher-order boundary conditions ($Du_1 = Du_2 = 0$, at $x_2 = 0, H$). The first higher-order boundary condition,

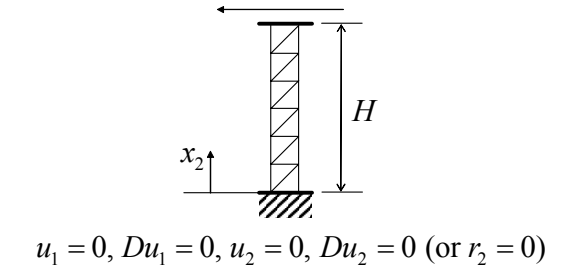

Figure 4.3: Illustration of a finite element mesh and boundary conditions for the simple shear problem using strain divergence elasticity.

$Du_1 = u_{1,2} = 0$, represents the perfect bonding between the face sheets and the core material, which was embodied into the discrete calculations by fixing the rotational degrees of freedom of the beam elements at the nodes where they connect to the face sheets (see Fig. 2.9). The second boundary condition, $Du_2 = u_{2,2} = 0$, however, is physically less clear. One could equally well prescribe the work-conjugate higher-order surface traction, $r_2 = 0$. In the following we will explore both possibilities.

The sample is taken to be infinitely long in the x_1 direction, and therefore, all field variables are independent of x_1. The kinematic variables are

$$\begin{aligned} &\varepsilon_{11} = 0, \quad \varepsilon_{22} = u_{2,2}, \quad \varepsilon_{12} = \frac{1}{2} u_{1,2}, \\ &\eta_1 = \varepsilon_{12,2} = \frac{1}{2} u_{1,22}, \quad \eta_2 = \varepsilon_{22,2} = u_{2,22}. \end{aligned} \tag{4.42}$$

In the absence of body forces, the equilibrium equations (4.19) reduce to

$$\sigma_{12,2} - \frac{1}{2} \tau_{1,22} = 0, \tag{4.43}$$

and

$$\sigma_{22,2} - \tau_{2,22} = 0. \tag{4.44}$$

Inserting the kinematics into the equilibrium equations via the constitutive equations (Equations (4.35) with $k = 0$) gives

$$l_c{}^2 u_{1,2222} - u_{1,22} = 0, \tag{4.45}$$

and

$$2 l_c{}^2 u_{2,2222} - \frac{C_{1111}}{A^{(1)}_{1212}} u_{2,22} = 0, \tag{4.46}$$

where l_c is the characteristic length defined as

$$l_c{}^2 = \frac{a}{A^{(1)}_{1212}}. \tag{4.47}$$

The solutions of these differential equations read

$$u_1 = C_1 + C_2 x_2 + C_3 e^{K_1 x_2} + C_4 e^{-K_1 x_2}, \tag{4.48}$$

and

$$u_2 = D_1 + D_2 x_2 + D_3 e^{K_2 x_2} + D_4 e^{-K_2 x_2}, \tag{4.49}$$

with $K_1 = 1/l_c$ and $K_2 = (C_{1111} / 2A_{1212}^{(1)})^{1/2} / l_c$. Incorporating the boundary conditions for u_1 yields

$$\begin{aligned}
C_1 &= \frac{\gamma H(e^{K_1 H} + e^{-K_1 H} - 2)}{4 - (2 - K_1 H)e^{K_1 H} - (2 + K_1 H)e^{-K_1 H}}, \\
C_2 &= \frac{\gamma HK(e^{-K_1 H} - e^{K_1 H})}{4 - (2 - K_1 H)e^{K_1 H} - (2 + K_1 H)e^{-K_1 H}}, \\
C_3 &= \frac{\gamma H(1 - e^{-K_1 H})}{4 - (2 - K_1 H)e^{K_1 H} - (2 + K_1 H)e^{-K_1 H}}, \\
C_4 &= \frac{\gamma H(1 - e^{K_1 H})}{4 - (2 - K_1 H)e^{K_1 H} - (2 + K_1 H)e^{-K_1 H}}.
\end{aligned} \tag{4.50}$$

For u_2, both choices of the higher order boundary conditions, $u_{2,2} = 0$ or $r_2 = 0$ at $x_2 = 0$ and H, give the same result:

$$D_1 = D_2 = D_3 = D_4 = 0 \Rightarrow u_2 = 0. \tag{4.51}$$

The non-vanishing tractions at the top surface of the sample are

$$t_1 = \frac{A_{1212}^{(1)}}{2} u_{1,2} - \frac{1}{2} a u_{1,222} \quad \text{and} \quad r_1 = \frac{1}{2} a u_{1,22}. \tag{4.52}$$

Since the work-conjugate to r_1, Du_1, is zero on the surface, the external work per unit out-of-plane thickness is done solely by t_1 and reduces to

$$W^{ex} = \int_S t_1 u_1 \, \mathrm{d}S = \gamma HGL l_c^{\,2} u_{1,222}, \tag{4.53}$$

where L is the width of the sample and $A_{1212}^{(1)} = 2G$ has been substituted. Note that from Equations (4.48) and (4.50) it follows that in the limit that l_c goes to zero, W^{ex} converges to $HGL\gamma^2$, the solution for the classical problem.

By comparing the governing equations and boundary conditions of the shear problem for strain divergence theory (see above) and couple stress theory (see Equations (3.38) and (3.39)), it follows that the displacement fields and overall response are identical, provided that

$$l_{\mathrm{c}}^{\text{Strain Divergence}} = \frac{l_{\mathrm{c}}^{\text{Couple Stress}}}{\sqrt{2}} . \tag{4.54}$$

In chapter 3, we have shown that the couple stress theory is able to successfully predict the local and global response for the analyzed discrete structures under simple shear, yielding specific values for the characteristic couple stress length. Therefore, the characteristic strain divergence length can be directly obtained from Equation (4.54).

In Figures 4.4a and b, we show the convergence for the linear and the quadratic finite elements implemented in the previous section, respectively. We compare the normalized shear strain $\varepsilon_{12}/\varepsilon_{12}'$ ($\varepsilon_{12}'=-\gamma/2$) through the thickness of a sample with $H/d=10$ and $l_{\mathrm{c}}/d=0.64$, for the analytical and finite element solutions (d is the cell size). The finite element mesh is shown in Fig. 4.3. The vertical displacements along the sides of the column are constrained to be zero. The penalty factor k in Equation (4.35) needed to constrain the relaxed displacement gradients ϕ_{ij} to be equal to $u_{i,j}$ was found be at least $50A_{1212}^{(1)}$. To trace the convergence, we gradually increase the number of elements in the x_2 direction (NE). Both linear and quadratic elements give a converged solution with increasing NE, with the convergence rate being much larger for the quadratic element.

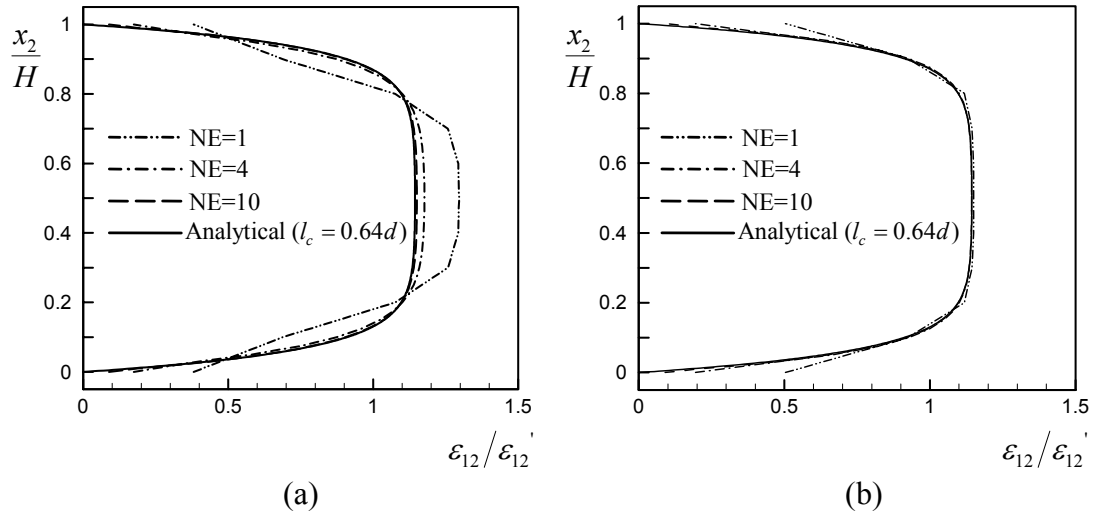

Figure 4.4: Convergence study for (a) the linear and (b) the quadratic elements. The normalized shear strain $\varepsilon_{12}/\varepsilon_{12}'$ ($\varepsilon_{12}'=-\gamma/2$) through the thickness of a sample with $H/d=10$ and $l_{\mathrm{c}}/d=0.64$ is plotted for an increasing number of elements in the x_2 direction (NE).

4.5 Analytical solution of the pure bending problem

In this section, we will solve the pure bending problem for the strain divergence theory[1]. The midplane of the plate is set as the x_1-x_3 plane, the x_3 direction coinciding with the out-of-plane direction (see Fig. 3.9). The pure bending assumption states that "transverse plane sections (that are parallel to the x_2-x_3 plane, in our case) remain plane and normal to the longitudinal fibres". A direct consequence of this is that the shear strains ε_{12} are zero throughout the beam. The most general displacement field that satisfies this can be written as

$$u_1 = \frac{1}{R} x_1 x_2, \;\; u_2 = -\frac{1}{2R} x_1^{\,2} + f(x_2) + P, \;\; u_3 = 0, \tag{4.55}$$

where f is a function of x_2 alone and P is an integration constant. The corresponding non-vanishing in-plane strains and strain divergence are

$$\varepsilon_{11} = \frac{1}{R} x_2, \;\; \varepsilon_{22} = f_{,2}, \;\; \text{and} \;\; \eta_2 = f_{,22}. \tag{4.56}$$

By inserting (4.56) into the constitutive equations (Equations (4.35) with $k = 0$), the non-vanishing in-plane stresses and higher-order stress are found as

$$\begin{aligned} \sigma_{11} &= C_{1111} \frac{x_2}{R} + C_{1122} f_{,2}, \\ \sigma_{22} &= C_{1111} f_{,2} + C_{1122} \frac{x_2}{R}, \\ \tau_2 &= 2a f_{,22}. \end{aligned} \tag{4.57}$$

The only non-trivial in-plane equilibrium equation is

$$\sigma_{22,2} - \tau_{2,22} = 0, \tag{4.58}$$

which combines with Equation (4.57) to yield the governing differential equation

$$2a f_{,2222} - C_{1111} f_{,22} - C_{1122} \frac{1}{R} = 0. \tag{4.59}$$

[1] See the Appendix for a summary of the bending solution for the strain gradient theory.

The solution of (4.59) reads

$$f = \frac{2a}{C_{1111}} \left(q_1 e^{\sqrt{\frac{C_{1111}}{2a}} x_2} + q_2 e^{-\sqrt{\frac{C_{1111}}{2a}} x_2} \right) - \frac{1}{2R} \frac{C_{1122}}{C_{1111}} {x_2}^2 + q_3 x_2 + q_4. \qquad (4.60)$$

If we merge the two constants q_4 in Equation (4.60) and P in Equation (4.55) into a single constant B, we have four unknowns (q_1, q_2, q_3, B) to be determined from the boundary conditions. The tractions at the top and the bottom surfaces are zero, yielding the (non-trivial) boundary conditions

$$\begin{aligned} t_2 &= \pm(\sigma_{22} - \tau_{2,2}) = 0 \quad \text{at} \quad x_2 = \pm H/2\,, \\ r_2 &= \tau_2 = 0 \quad \text{at} \quad x_2 = \pm H/2\,. \end{aligned} \qquad (4.61)$$

The first two equations ($t_2 = 0$ at $\pm H/2$) are not linearly independent, which leaves only 3 independent equations. The fourth equation comes from specifying the displacement u_2 to be zero at $x_1 = x_2 = 0$. Solving the four equations for the four unknowns yields

$$q_1 = q_2 = -\frac{BC_{1111}}{4a} = \frac{C_{1122} e^{\sqrt{\frac{C_{1111}}{8a}} H}}{C_{1111} R \left(e^{\sqrt{\frac{C_{1111}}{2a}} H} + 1 \right)}, \quad q_3 = 0. \qquad (4.62)$$

Now that we know the displacement fields, we can calculate the macroscopic bending moment by using the external work expression (4.18). The line force s_i acting at the sharp out-of-plane edges of a cross-section perpendicular to the length of the beam follows from Equation (4.21) to be $(s_1, s_2, s_3) = (\tau_2/2,\ \tau_1/2,\ 0)$ at $x_2 = H/2$ and $(s_1, s_2, s_3) = (-\tau_2/2,\ -\tau_1/2,\ 0)$ at $x_2 = -H/2$. The component of the edge force that does work is s_1, but since $\tau_2 = 0$ is prescribed at the top and bottom surfaces, this contribution vanishes. As a result, the bending moment per unit out-of-plane thickness can be written as

$$M = \int_{-H/2}^{H/2} x_2 \sigma_{11}\, \mathrm{d}x_2 - \frac{1}{2} \int_{-H/2}^{H/2} (x_2 \tau_{2,2} + \tau_2)\, \mathrm{d}x_2. \qquad (4.63)$$

The second integral in Equation (4.63) vanishes irrespective of the material parameters and we are left with

$$M = \int_{-H/2}^{H/2} x_2 \sigma_{11} \, \mathrm{d}x_2. \tag{4.64}$$

This expression has exactly the same form as the classical bending moment. In the strain divergence theory, however, the vertical displacement field u_2 differs from that in classical elasticity due to the higher-order boundary conditions at the traction-free top and bottom surfaces. As a result, σ_{11} as given in Equations (4.57), is non-linear over the cross-section. In the following we will analyze the difference between the strain divergence and the classical solution for isotropic and transverse isotropic materials, for which the material constants C_{1111} and C_{1122} in Equations (4.57) follow from Equations (3.19) and (3.17), respectively. The ratio of σ_{11} for the strain divergence theory, ${\sigma_{11}}^{\mathrm{SD}}$, to the corresponding one for the classical continuum theory, ${\sigma_{11}}^{\mathrm{C}}$, can be written for isotropic materials as

$$\frac{{\sigma_{11}}^{\mathrm{SD}}}{{\sigma_{11}}^{\mathrm{C}}} = 1 + \frac{(1 - f_{,2} / {\varepsilon_{22}}^{\mathrm{C}})\nu^2}{1 - 2\nu}, \tag{4.65}$$

and for transverse isotropic materials (with a zero out-of-plane Poisson's ratio, $\nu_{\mathrm{pt}} = 0$), as

$$\frac{{\sigma_{11}}^{\mathrm{SD}}}{{\sigma_{11}}^{\mathrm{C}}} = \frac{1 - (f_{,2} / {\varepsilon_{22}}^{\mathrm{C}}){\nu_{\mathrm{p}}}^2}{1 - {\nu_{\mathrm{p}}}^2}. \tag{4.66}$$

Here, ${\varepsilon_{22}}^{\mathrm{C}}$ is the classical strain field and ν_{p} the in-plane Poisson's ratio. Note that $f_{,2}/{\varepsilon_{22}}^{\mathrm{C}}$ depends on the Poisson's ratio and the characteristic length. For a vanishing characteristic length, f falls back onto its classical counterpart (see Equation (4.60)), as it should be. For zero Poisson's ratio, ${\sigma_{11}}^{\mathrm{SD}}/{\sigma_{11}}^{\mathrm{C}} = 1$, irrespective of the value for the characteristic length. Figure 4.5a and b show $f_{,2}/{\varepsilon_{22}}^{\mathrm{C}}$ and ${\sigma_{11}}^{\mathrm{SD}}/{\sigma_{11}}^{\mathrm{C}}$, respectively, plotted against the normalized distance from the neutral axis, $2x_2/H$, on the upper half of the beam, for a transverse isotropic material with a characteristic length of $l_{\mathrm{c}} = 0.64d$ and for $H = 2d$. We see that $f_{,2}/{\varepsilon_{22}}^{\mathrm{C}}$ is between 0.3 and 0.4 for $\nu_{\mathrm{p}} = 0$ and converges to one as the value of ν_{p} approaches the incompressibility limit $\nu_{\mathrm{p}} = 1$. ${\sigma_{11}}^{\mathrm{SD}}/{\sigma_{11}}^{\mathrm{C}}$, on the other hand, is constant and equal to one throughout the whole beam for ν_{p} equal to zero. With increasing ν_{p}, the ratio increases uniformly over the cross-section until $\nu_{\mathrm{p}} \approx 0.7$. With a further increase of ν_{p}, ${\sigma_{11}}^{\mathrm{SD}}/{\sigma_{11}}^{\mathrm{C}}$ increases towards the top surface and falls back to one in the middle of the beam. For ν_{p} approaching the incompressibility limit, $\nu_{\mathrm{p}} = 1$, its value gets very large in a small region close to the top surface (${\sigma_{11}}^{\mathrm{SD}}/{\sigma_{11}}^{\mathrm{C}} = 46$ at $\nu_{\mathrm{p}} = 0.9999$). The tendencies are the same in the case of isotropic solids, and will not be shown here.

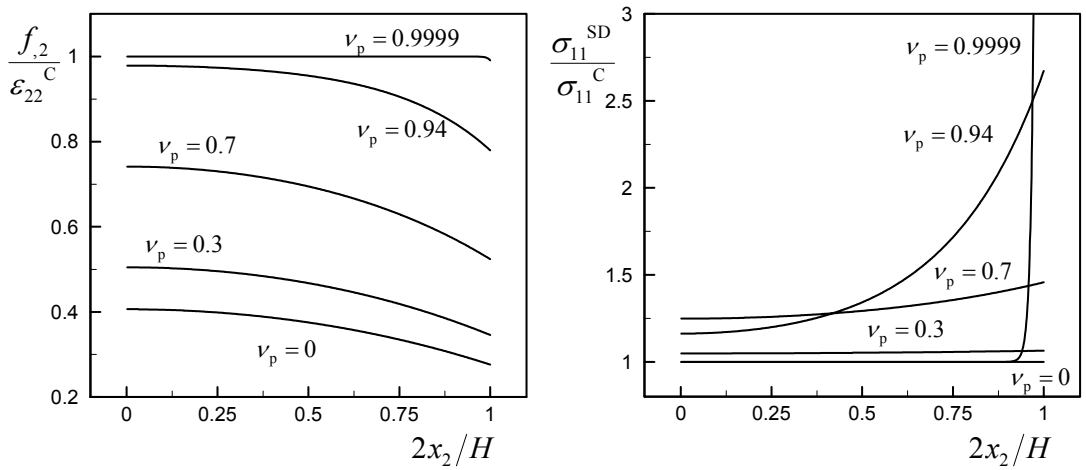

Figure 4.5: The ratio of (a) the transverse strain ($f_{,2}$) and (b) the normal stress ($\sigma_{11}{}^{SD}$) given by the strain divergence theory to their classical counterparts ($\varepsilon_{22}{}^{C}$ and $\sigma_{11}{}^{C}$, respectively), for transverse isotropic materials with a characteristic length of $l_c = 0.64d$, a height of $H = 2d$ and with different Poisson's ratios ranging from $\nu_p = 0$ to $\nu_p \approx 1$.

Multiplication of the bending moment with the radius of curvature R yields the bending stiffness. The bending stiffness of a classical isotropic continuum beam is

$$B_{\text{class}} = \frac{EH^3}{12(1-\nu^2)}. \tag{4.67}$$

To be able to write the normalized bending stiffness in a more convenient way, we will introduce a function $g(x_2)$ such that

$$g(x_2) = f(x_2)_{,2} + \frac{1}{R}\frac{C_{1122}}{C_{1111}}x_2. \tag{4.68}$$

Then, the normalized bending stiffness can be written as

$$\frac{B}{B_{\text{class}}} = 1 + \frac{12R\nu(1-\nu)}{(1-2\nu)H^3}\int_{-H/2}^{H/2} x_2 g \, \mathrm{d}x_2. \tag{4.69}$$

The corresponding solution for the transverse isotropic case (with a zero out of plane Poisson's ratio, $\nu_{pt} = 0$), can be find in a similar manner as

$$\frac{B}{B_{\text{class}}} = 1 + \frac{12R\nu_p}{(1-\nu_p{}^2)H^3}\int_{-H/2}^{H/2} x_2 g \, \mathrm{d}x_2, \tag{4.70}$$

with the classical bending stiffness defined as

$$B_{\text{class}} = \frac{E_{\text{p}} H^3}{12} . \tag{4.71}$$

Figure 4.6 shows the normalized bending stiffness plotted as a function of the normalized height H/d, for an increasing Poisson's ratio for the couple stress theory (Equation (3.48)) and the strain divergence theory (Equation (4.70)). The characteristic length is taken to be the one obtained by fitting the continuum results of the shear problem to the corresponding discrete results of the Voronoi microstructures: $l_{\text{c}}^{\text{CS}} = 0.9d$ (corresponding to $l_{\text{c}}^{\text{SD}} = 0.64d$). We see that there is stiffening in the small H/d regime for both cases. The stiffening increases with increasing Poisson's ratio for the strain divergence case, whereas it decreases for the couple stress theory. For the same Poisson's ratio, the stiffening is larger for the couple stress solid, but the difference vanishes as we approach to the incompressibility limit $\nu_{\text{p}} = 1$. For Poisson's ratio's smaller than, say, $\nu_{\text{p}} < 0.7$, the stiffening for the strain divergence solution is small, whereas it is quite high for the couple stress solution.

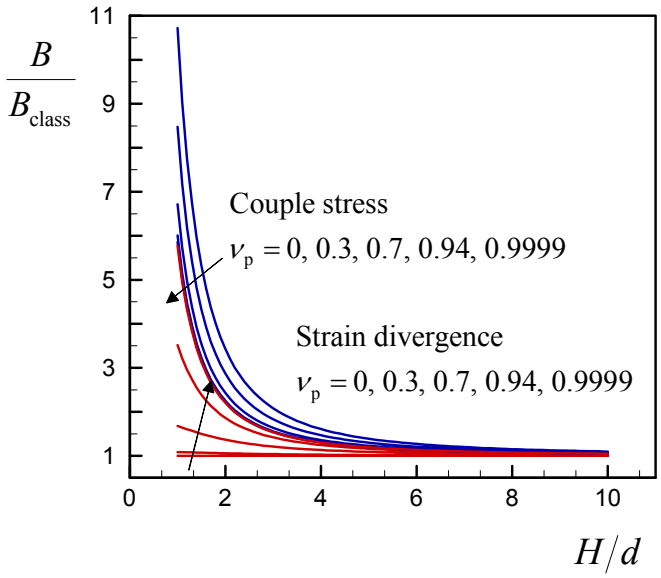

Figure 4.6: The normalized bending stiffness plotted as a function of the normalized height H/d, for an increasing Poisson's ratio, for the couple stress (in blue) and strain divergence (in red) theories. The arrows denote the direction of increasing ν_{p}.

4.6 Summary and conclusions

In this chapter we developed a higher-grade continuum theory that falls in the class of Toupin-Mindlin's strain gradient theories. The theory incorporates the divergence of strain to be the additional higher-grade kinematic measure. Fist, we derived the equilibrium equations and the boundary conditions for the strain divergence theory. We developed a finite element implementation of the theory making use of the penalty approach. Then, we solved the simple shear problem analytically and assessed the accuracy of the finite element method. The strain divergence and couple stress theory turn out to yield the same solution for the simple shear problem, provided that the characteristic length for the strain divergence solid l_c^{CS} is related to the characteristic length for the couple stress solid l_c^{CS} via $l_c^{SD} = l_c^{CS}/\sqrt{2}$.

In the plane strain bending of a classical solid, ε_{22} varies linearly through the thickness of the beam. In the case of a strain divergence solid, however, ε_{22} becomes non-linear (i.e. exponential) as a result of satisfying both the classical and additional higher-order boundary conditions. This difference in ε_{22} results in an increasing bending stiffness with decreasing specimen thickness, being larger for larger Poisson's ratios. Nevertheless, for the same Poisson's ratio, the stiffening of a strain divergence solid is less than the stiffening of a couple stress solid, with this difference being larger when the Poisson's ratio is low.

Appendix: Pure bending for the strain gradient theory

In this appendix we summarize the analytical solution of the plane-strain pure bending problem for Toupin-Mindlin's strain gradient theory. The geometry of the problem is shown earlier in Fig. 3.9. The displacement field that satisfies the pure bending assumption for the strain gradient elasticity is the same as given for the strain divergence theory in Equations (4.55). The corresponding non-vanishing in-plane strains and strain gradients (see Equations (1.13)) are

$$\begin{aligned} &\varepsilon_{11} = \frac{1}{R}\, x_2, \;\; \varepsilon_{22} = f_{,2}, \\ &\eta_{211} = \frac{1}{R} \;\text{ and }\; \eta_{222} = f_{,22}. \end{aligned} \tag{A1}$$

By inserting (A1) into the constitutive equations (1.15), the non-vanishing in-plane stresses and higher-order stresses are found as

$$\begin{aligned} \sigma_{11} &= C_{1111}\, \frac{x_2}{R} + C_{1122} f_{,2}, \\ \sigma_{22} &= C_{1111} f_{,2} + C_{1122}\, \frac{x_2}{R}, \\ \tau_{112} &= \left(\frac{1}{2}\, a_1 + a_5 \right) \frac{1}{R} + \left(\frac{1}{2}\, a_1 + a_3 \right) f_{,22}, \\ \tau_{211} &= \left(a_2 + a_4 \right) \frac{2}{R} + \left(a_1 + 2a_2 \right) f_{,22}, \\ \tau_{222} &= \left(a_1 + 2a_2 \right) \frac{1}{R} + 2 \left(a_1 + a_2 + a_3 + a_4 + a_5 \right) f_{,22}. \end{aligned} \tag{A2}$$

The only non-trivial in-plane equilibrium equation is

$$\sigma_{22,2} - \tau_{222,22} = 0, \tag{A3}$$

which combines with (A2) to yield the governing differential equation

$$2(a_1 + a_2 + a_3 + a_4 + a_5) f_{,2222} - C_{1111} f_{,22} - C_{1122}\, \frac{1}{R} = 0. \tag{A4}$$

The solution of (A4) reads

$$f = \frac{2a_{\mathrm{h}}}{C_{1111}}\left(q_1 e^{\sqrt{\frac{C_{1111}}{2a_{\mathrm{h}}}}x_2} + q_2 e^{-\sqrt{\frac{C_{1111}}{2a_{\mathrm{h}}}}x_2} \right) - \frac{1}{2R}\frac{C_{1122}}{C_{1111}} {x_2}^2 + q_3 x_2 + q_4, \qquad \text{(A5)}$$

where $a_{\mathrm{h}} = a_1 + a_2 + a_3 + a_4 + a_5$. Combining the two constants q_4 in Equation (A5) and P in Equation (4.55) into a single constant B, we have four unknowns (q_1, q_2, q_3, B) to be determined from the boundary conditions. The non-trivial traction boundary conditions at the top and the bottom surfaces are

$$\begin{aligned} t_2 &= \pm(\sigma_{22} - \tau_{222,2}) = 0 \quad \text{at} \quad x_2 = \pm H/2\,, \\ r_2 &= \tau_{222} = 0 \quad \text{at} \quad x_2 = \pm H/2\,. \end{aligned} \qquad \text{(A6)}$$

The first two equations ($t_2 = 0$ at $\pm H/2$) are not linearly independent, which leaves only 3 independent equations. The fourth equation comes from specifying the displacement u_2 to be zero at $x_1 = x_2 = 0$. Solving the four equations for the four unknowns yields

$$q_1 = q_2 = -\frac{BC_{1111}}{4a_h} = -\frac{(a_1 + 2a_2)C_{1111} - 2a_{\mathrm{h}}C_{1122}e^{\sqrt{\frac{C_{1111}}{8a_h}}H}}{2a_{\mathrm{h}}C_{1111}R\left(e^{\sqrt{\frac{C_{1111}}{2a_h}}H} + 1 \right)}, \quad q_3 = 0. \qquad \text{(A7)}$$

In the case of the strain gradient elasticity, the line forces s_k acting at the sharp edges read

$$s_k = z_j n_i \tau_{ijk}, \qquad \text{(A8)}$$

which reduce to $(s_1, s_2, s_3) = (\tau_{112} + \tau_{211}, 0, 0)$ at $x_2 = H/2$ and $(s_1, s_2, s_3) = (-\tau_{112} - \tau_{211}, 0, 0)$ at $x_2 = -H/2$ for the out-of-plane edges of a cross-section perpendicular to the length of the beam. By inserting these and the (higher-order) tractions in the external work expression (4.18), the macroscopic bending moment per unit out-of-plane thickness can be written as

$$\begin{aligned} M = &\int_{-H/2}^{H/2} x_2 \sigma_{11}\, \mathrm{d}x_2 - \int_{-H/2}^{H/2} \left(x_2(\tau_{211,2} + \tau_{112,2}) + \tau_{112} \right) \mathrm{d}x_2 \\ &+ \frac{H}{2}\left(\tau_{112}\,|_{x_2 = H/2} + \tau_{211}\,|_{x_2 = H/2} \right) + \frac{H}{2}\left(\tau_{112}\,|_{x_2 = -H/2} + \tau_{211}\,|_{x_2 = -H/2} \right). \end{aligned} \qquad \text{(A9)}$$

Multiplying the bending moment with the radius of curvature R yields the bending stiffness.